

[T2.1] Characterizing Shortest-Path Ensembles for Brain Network Modeling Using Empirical Constraints

Daniel Peña Fonseca and Lukas Prader
(Dated: January 8, 2026)

Understanding how anatomical pathways facilitate the flow of information in the human brain remains a fundamental challenge in network neuroscience. Several network communication models have been proposed to describe communication between brain regions. Parametric models, particularly shortest path ensembles, provide a simulation framework lying between optimal routing regimes and diffusion regimes of network communication by using a set of k alternatives (near-shortest paths). The number k that would best approximate empirical results remains unknown. Using structural connectomes and then simulating signal outputs over time, this report addresses this question by varying the number of paths considered to determine which range minimizes discrepancies between empirical data (connectomes and functional MRIs) and simulated results. Our results suggest that $k \approx 8$ may be most relevant for brain communication, although correlations are weak and need further investigation.

Project Topic: Brain Network Modelling

Teaching Assistant: Yu-Wei Chang

I. INTRODUCTION

Understanding how information propagates between brain regions is a central challenge in neuroscience. It is believed that the large range of connectivity patterns and dynamic properties exhibited by the human brain are central for information processing and complex behavior [1].

It has been shown that brain structure exhibits characteristic properties such as small-world topology, combining high local clustering with additional long-range connections [2]. The network also contains highly connected hub regions, creating a structure supporting long-range communication, essential for efficient information propagation [3]. These results paved the way for graph-based network models of the brain, balancing local processing and efficient long-range communication between functionally separated brain regions [4].

Structural connectivity (SC), measuring the strength of white matter connections between brain regions; and functional connectivity (FC), the correlation of brain activity time series between ROIs, are two measurements which allow researchers to investigate brain dynamics and build models of brain communication. While multiple studies have shown significant statistical relationships between SC and FC, there are also several cases of strong functional relationships of regions with no direct structural connection [5].

Brain network communication models propose mechanisms for signal transmission through the connectome, abstracting biological neural signaling to network communication [4]. Models often use one of two communication paradigms: optimal network routing, where signals follow the most efficient (shortest) path, or diffusive dynamics, where information flows stochastically according to local connectivity [4].

However, both extremes capture only certain aspects of real neural communication, and place assumptions about

the nature of information flow. In shortest-path routing, signals are assumed to have full knowledge of the global network structure, while diffusive models assume that regions have only local information to guide communication [4]. Brain network topology achieves a balance between diffusion and routing efficiency due to the highly connected hubs present in the connectome [1].

Parametric models operate on the continuum between the diffusive and shortest-path routing extremes [4], striking a trade-off between transmission cost and information cost. Additionally, studies have shown that including alternative pathways can improve efficiency and strengthen robustness and resilience in brain networks [1], which are additional factors to consider for realistic models of neural communication.

Despite these insights, major gaps remain. In particular, there is no consensus over which kinds of paths or how many should be used for a signal to travel between ROIs. Seeking to answer these questions, in this study we investigate information transfer using a parametric model. Using simulations based on structural connectomes, we intend to capture which parameter values most accurately reflect empirical patterns of brain activity.

II. OVERVIEW

Connectome data can be used to simulate brain activity based on a range of brain network communication models [4]. When wanting to explore how available information impacts the performance of communication models, parametric models provide a flexible framework. They enable specific parameter tuning, which can give insights into how strongly different trade offs (e.g. efficiency vs transmission cost) should be considered to match empirical observations. Examples of this type of framework include linear threshold models [6], biased random walks [7] and shortest path ensembles [8]. A com-

Table I: **Overview of parametric network communication models.** List of three potentially viable models and a description of their characteristics.

Method / Model	Use case scenario	Features	Suitable for the project?
Linear threshold model	Looking at signal propagation over time, influenced by local neighborhood activation	Neighbor transmission threshold	Can characterize communication models based on transmission time and neighborhood topology
Biased random walk	Investigating the impact of structural information on random walk dynamics	Transition bias, amount of structural information allowed to influence random transitions	Classifies models by the amount of structural information necessary to select paths compared to random walks
Shortest path ensembles	Analyzing behavior related to deviations from optimal path signaling	Number of shortest paths k	Differentiates models simply by the number of most optimal paths allowed for communication

mon property among them is their ability to tune how far the model should lean towards diffusion-type models or shortest-path approaches by changing parameters.

In order to determine the method most suitable for our research question, the features and specific use case scenarios for each of them need to be compared (see Table I).

Method 1 (Linear threshold models). In this approach, signal propagation is determined by the number of neighboring nodes that have already received the signal [6]. Each node in the network will receive the information only if a proportion of more than θ of its neighbors has previously received the transmission, making θ the tunable parameter of the model. With $\theta = 0$, each node with at least one activated neighbor will receive the signal, resulting in maximal diffusion through broadcasting [4]. Increasing θ , the conditions for activation become progressively stricter, reducing the propagation throughout the network. For θ sufficiently large, information flow can reach a bottleneck, reflecting a regime in which only tightly clustered neighborhoods can participate in transmission.

Method 2 (Biased random walks). In unbiased random walks, the probability of a signal propagating from node i to node j is proportional to the connection weight between these nodes [9]. Alternatively, in biased random walks, transition probabilities are additionally influenced by the amount of global topological information available to individual nodes [7]. This is controlled by the tunable parameter λ . With $\lambda = 0$, unbiased random walks are recovered, since individual nodes will only possess information regarding their own connections. In contrast, for $\lambda \rightarrow \infty$, the biased random walk converges to the shortest path, since transmissions between any two nodes will make use of the entire global topological information, leading to optimal paths [4].

Method 3 (Shortest path ensembles (SPE)). This parametric model considers that signals between any two brain regions do not only travel along the most efficient route, but through one of the k most efficient (shortest) paths [8]. Standard shortest-path routing is recovered setting $k = 1$, while $k \rightarrow \infty$ implies diffusive communication since then all possible paths are consid-

ered for signaling. Small values of k would require extensive global topological knowledge of the network, while larger values of k would relax these conditions, resulting in smaller informational cost [4]. Since SPE is a relaxation of shortest path routing, many metrics and methods applicable to shortest path routing can be adapted to SPE.

All three methods can be considered suitable for the research question, as they allow to change the kinds of paths allowed for communication by varying their respective parameters.

Linear threshold models focus on the influence of local neighborhoods and the amount of time (steps) it takes for information to spread from one ROI to another. This makes them suitable to investigate the communication speed and efficiency of transmissions spreading over time.

Several metrics, like diffusion efficiency and search information, use random walks as their basis, making biased random walks suitable for studies centered around these metrics. They focus on the efficiency and accessibility of communication paths, linking global structural properties to functional connectivity.

SPEs are inherently more selective, as they focus on the most efficient paths and their near alternatives [4]. The model also derives a distance metric between ROIs, the k -shortest path length [8]. It intuitively describes how far regions are apart based on the weighted average of the k -shortest paths.

For this project, the SPE model was chosen. It allows the investigation of how many near optimal paths should be considered to best represent empirical data. The parameter k directly determines the number of paths considered, making it more interpretable than abstract metrics like search information or diffusion efficiency required as parameters for biased random walks. We were also not interested in time-resolved dynamics, making linear threshold models unsuitable.

III. METHOD

We developed a workflow (Fig. 1) to evaluate the performance of the SPE model while varying k . We simulate

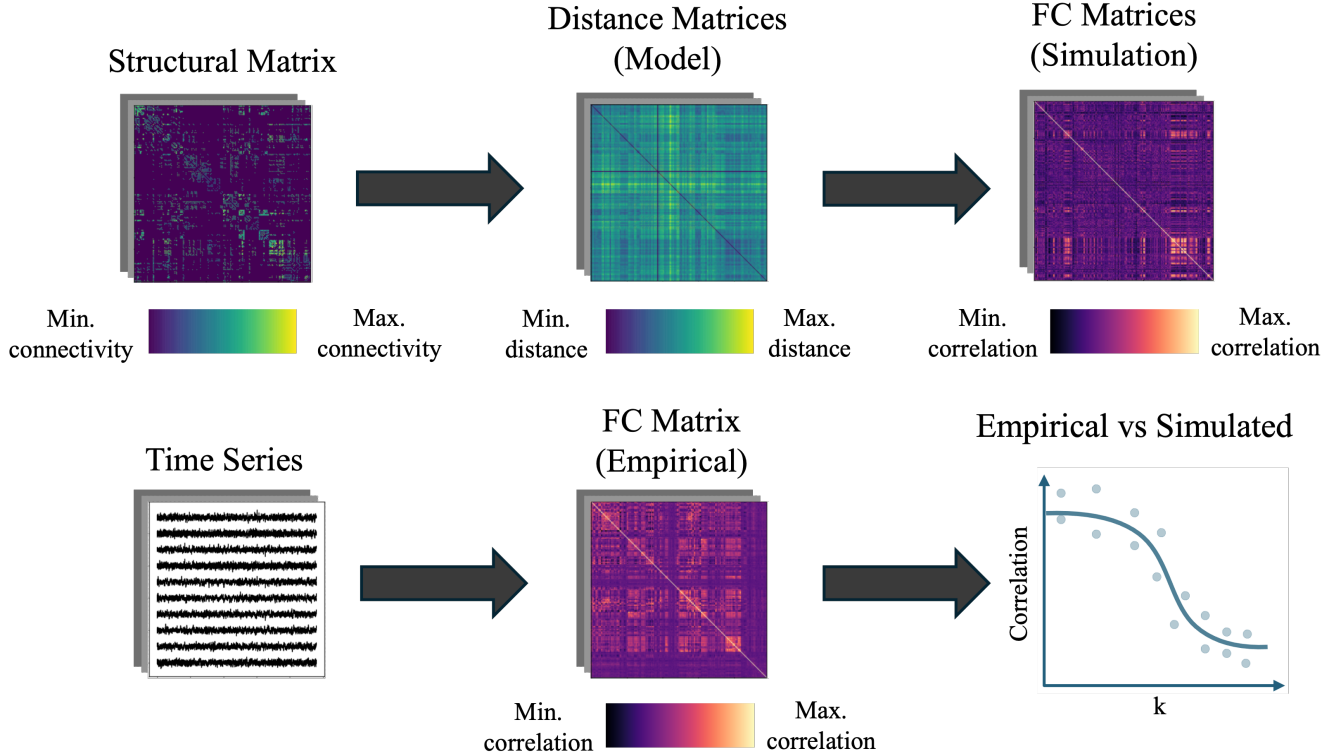


Figure 1: Method overview. The illustrated workflow summarizes the steps taken to simulate and evaluate the shortest-path ensemble model against empirical brain data for all patients. Structural connectivity matrices and fMRI time series from the provided dataset are used as inputs. SC matrices are used to derive the k -distance matrices for k ranging from 1 to 50. The obtained distance matrices are then used as coupling matrices in the Kuramoto model to simulate brain activity over time, resulting in simulated FC matrices. Empirical FC matrices are computed from the fMRI time series using Pearson correlation. Finally, the simulated FC matrices are compared to the empirical FC matrices using Pearson correlation to assess model performance across different values of k . (Bottom right illustration taken from [10]).

brain activity and compare it to empirical data using the Python programming language.

Dataset. The provided dataset contained structural connectivity (SC) matrices obtained with measurements using Diffusion Tensor Imaging (DTI) and time series from resting-state functional Magnetic Resonance Imaging (rfMRI) data from 100 healthy participants [11]. The measurements concerned 246 brain ROIs defined by the Brainnetome atlas [12].

The SC matrices are sparse, symmetric matrices of the mean fractional anisotropy (values between 0 and 1) between ROIs representing the connection strength between them (Fig. 2 A). The time series represent the averaged Blood Oxygen Level Dependent (BOLD) signal from each ROI, z-scored over time for each ROI and thus having mean 0 and standard deviation 1. Time steps of 0.72 seconds were used for 4800 measurements, which is equivalent to 57.6 minutes.

k -shortest path length. Making use of the SPE model, we computed the k -shortest path length [8] between every pair of ROIs for each patient.

For this, we calculated the edge lengths between ROIs as $l_{u,v} = -\log(w_{u,v})$, where $w_{u,v}$ is the connection weight between nodes u and v in the SC matrix. Using logarithmic transform creates edge lengths that increase the number of paths that are able to be incorporated in efficient communication.

The topological length $d(\pi_{u,v})$ of a path $\pi_{u,v}$ between nodes u and v is defined as the sum of the edge lengths of all edges $e_{i,j}$ along the path. The `scipy` [13] implementation of Yen's algorithm was used to compute the k shortest paths between every pair of ROIs, for k up to 50.

The k -shortest path length $D_k(s,t)$ between nodes s and t is then defined as the weighted average of the lengths of the k shortest paths between connecting s and t :

$$D_k(s,t) = \sum_k \hat{P}(\pi_{s,t}^k) d(\pi_{s,t}^k). \quad (1)$$

$\hat{P}(\pi_{s,t}^k)$ is the normalized probability $P(\pi_{s,t}^k)$ of the k -

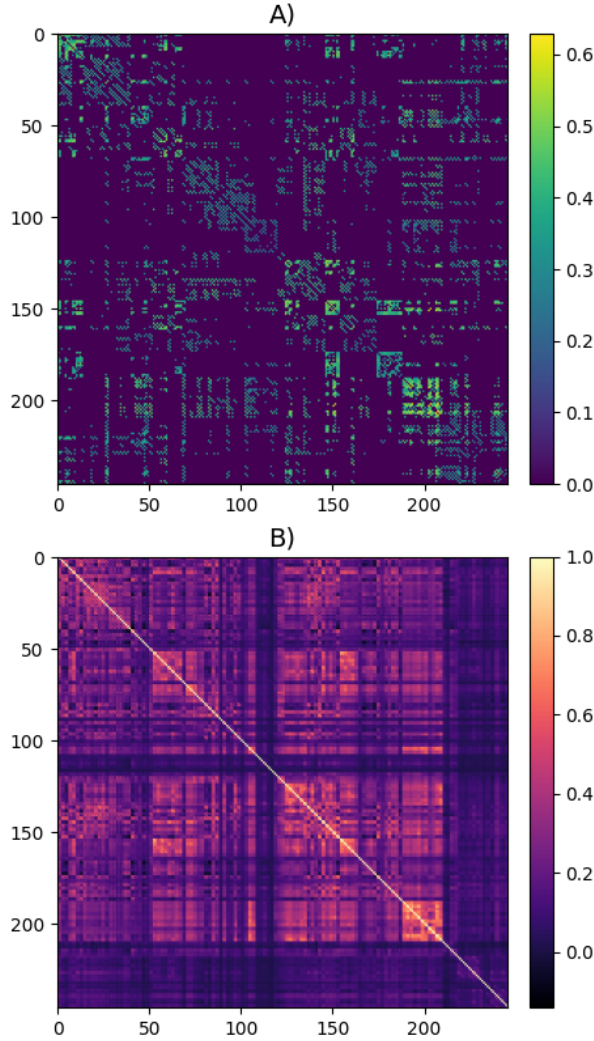


Figure 2: Averaged SC and FC matrix. Matrices showing the averaged structural connectivity (A) and functional connectivity (B) over all patients for illustration purposes. Color describes the connection strength or functional connectivity between two ROIs respectively.

shortest path $\pi_{s,t}^k$ being followed under random walk dynamics:

$$P(\pi_{s,t}^k) = \sum_{e_{u,v} \in \pi_{s,t}^k} \frac{w_{u,v}}{\sum_j w_{u,j}}. \quad (2)$$

$D_k(s, t)$ thus represents the combined distances of all k -shortest paths, weighted by their accessibility under random walk dynamics. For each patient and each value of k from 1 to 50, we obtained a k -distance matrix containing the k -shortest path lengths between every pair of ROIs.

Functional Connectivity (FC). Derived from ROI activity, functional connectivity describes the statistical relationships between ROI time series [1]. The simplest

way is to calculate the Pearson correlation coefficient between the time series of each pair of ROIs, resulting in a symmetric FC matrix (Fig. 2 B). For each patient, we calculated the empirical FC matrix from the provided fMRI time series and from the simulated ROI activity using Pearson correlation.

Kuramoto Model. In order to simulate brain activity based on the empirical brain structure, we decided to model the brain regions as a network of coupled Kuramoto oscillators. Although chosen for simplicity, it retains similar performance to more biophysical and realistic (i.e. neural mass) models [14], while still being more flexible than simple firing rate models, which use a decaying firing rate under influence of random noise and input from the network [15].

Defining $\theta(t)$ as the phase of oscillator (ROI) $n \in \{1, \dots, N\}$ at time t , the dynamics of the system are governed by the following equation [14]:

$$\frac{d\theta_n}{dt} = \omega_n + c \cdot \sum_{p=1}^N C_{np} \cdot \sin(\theta_p(t - \tau_{np}) - \theta_n(t)) + \eta_n(t). \quad (3)$$

The term ω_n represents the intrinsic angular frequency of ROI n , satisfying $\omega_n = 2\pi f_n$, where f_n is sampled from a fixed Gaussian distribution with mean $f_0 = 60\text{Hz}$ and standard deviation $\sigma_f = 5$ at the beginning of the simulation. C_{np} is the relative coupling strength from node p to node n , and c is the global coupling strength, which scales all connection strengths. The delay in transmissions from p to n is incorporated through τ_{np} , which depends on the distance between the nodes. Defining L_{np} as one element of the network distance matrix L , and the average distance between nodes as $\langle L \rangle$, the delay is defined as $\tau_{np} = \langle \tau \rangle L_{np} / \langle L \rangle$, with $\langle \tau \rangle = 11\text{ms}$. Lastly, $\eta_n(t)$ represents noise present in the network, implemented as Gaussian white noise with mean 0 and standard deviation $\sigma_n = 3$. All parameter values were taken from [14].

In our case, the distance matrix L is one of the k -distance matrices, while the coupling matrix C , also called adjacency matrix, is calculated using $C_{np} = 1/L_{np} \forall n, p$.

This framework allowed us to simulate brain activity time series for each patient and each value of k , evolving the phases of all ROIs over time and ultimately obtaining activity time series by calculating $\sin(\theta_n(t))$.

Simulation. Due to the high computational cost of simulating the systems, we only simulated for a selection of k values, namely $k \in \{1, 2, \dots, 10, 25, 35, 50\}$. Simulations were performed for 5 seconds using a time step of 0.1 ms. FC matrices were calculated from the simulated activity after removing the first 500 ms to allow the system to stabilize.

Evaluation. In order to evaluate the SPE model performance, we calculated the Pearson correlation between the upper triangle elements, excluding the diagonal. These correlations were then analyzed to determine the best performing k values on a mean and per-patient

basis. To check for significant differences between different k values, Analysis of Variance (ANOVA) tests were performed, which check if the distributions between samples (here all simulations for a particular k) are significantly different.

Parameter Optimization. The global coupling strength c needs to be of the correct scale to ensure stability and validity of the system [14]. With more connections in the coupling matrix, the value of c has to be smaller [15]. Ref. [14] proposes a value of $c = 18$ when using SC matrices with 66 ROIs as adjacency matrices. Since our coupling matrices have 246 ROIs and are not directly comparable to SC matrices, we performed a parameter sweep to find the optimal scaling factor s for $c = s \cdot 18$. For a particular value of s , simulations of 2 seconds using a step size of 0.1 ms were performed for $k = 1, 5, 10, 30$ with three repetitions each. Upper triangle Pearson correlations were calculated between simulated and empirical FC matrices and then averaged over all k and repetitions to get a performance value.

Initial tests suggested the performance function to have a unimodal maximum, which is why it was decided to optimize s by minimizing the negative performance function with a `scipy` [13] implementation of Brent's method in the bounded interval $[0.05, 1]$, iterating for 10 steps. It uses a combination of bisection, secant method and parabolic interpolation to find the minimum of a function without requiring derivatives, making it suitable for our optimization problem where the performance function may not be smooth or differentiable.

IV. RESULTS AND DISCUSSION

Figure 3 shows three example k -distance matrices ($k = 1, 5, 25$), obtained by averaging over all patients. It can be seen that for increasing values of k , the matrices become more uniform in color. This suggests that once many paths are considered, ROIs become more similar in terms of their k -distance, as signals can propagate through many alternative routes, creating a diffusive regime. For lower values of k , the matrices show more structure like regions with low distance values, indicating that certain ROIs form well connected clusters, i.e. the regions around the index 150 and 200 in the matrices (Fig. 3, top).

To show how the structure of the k -distance matrices relates to empirical functional connectivity, the Pearson correlation between both matrices was calculated for each patient. Averaging the results over all patients, the mean correlation and its standard deviation were then represented as a function of k (Fig. 4).

The first thing to notice is the negative sign of the correlation values. Since we correlate distance with functional connectivity, this implies that ROIs with higher k -distance between them exhibit lower functional connectivity. One can also observe clear k -dependence, with the strongest mean correlation being $r \approx -0.129$ at $k = 1$,

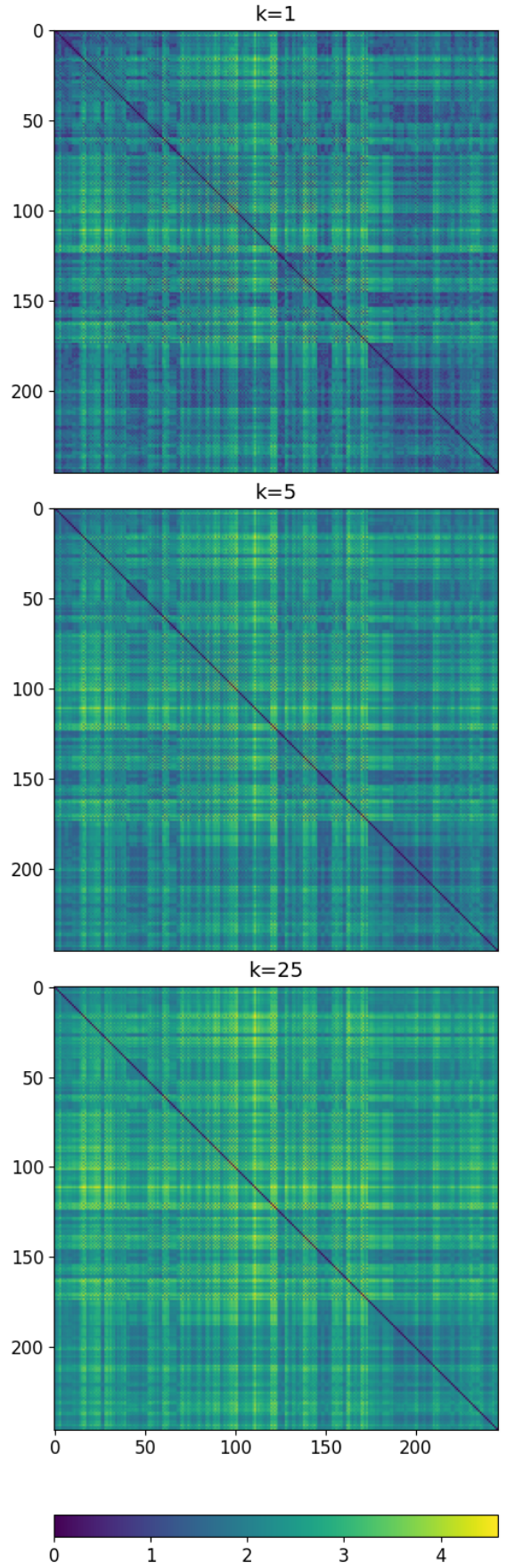


Figure 3: **Example k -distance matrices.** Three k -distance matrices showing $k=1$ (top), $k=5$ (middle) and $k=25$ (bottom), obtained by averaging over all patients. Color describes the k -shortest path length (Eq. 1) between two ROIs.

which only uses shortest path routing. For $k > 1$ correlation is weaker, but has a stable plateau with $r \approx -0.125$ up to $k = 10$, after which correlation decreases further, reaching $r \approx -0.1$ at $k = 50$. This suggests that additional paths, if close to the shortest path, relate differently to functional connectivity than longer paths. The scale of the standard deviation indicates that there is considerable variability between patients, yet ANOVA confirms significant differences between the distributions of each k with $p \ll 0.001$.

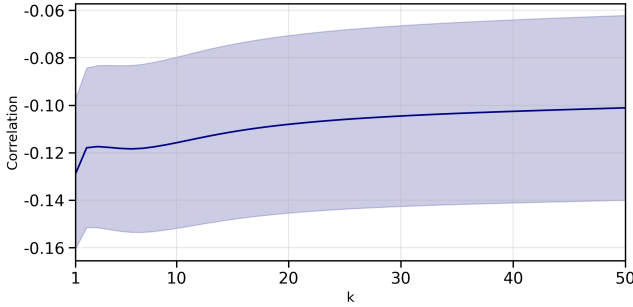


Figure 4: Correlation of k -distance matrices and empirical FC. Pearson correlation between k -distance matrices and empirical FC matrices for all patients, shown as mean with standard deviation as error band.

The optimization of the scaling factor s scaling the global coupling strength c is shown in Figure 5, with the maximal correlation between simulated and empirical FC achieved with a scaling factor $s \approx 0.2098$.

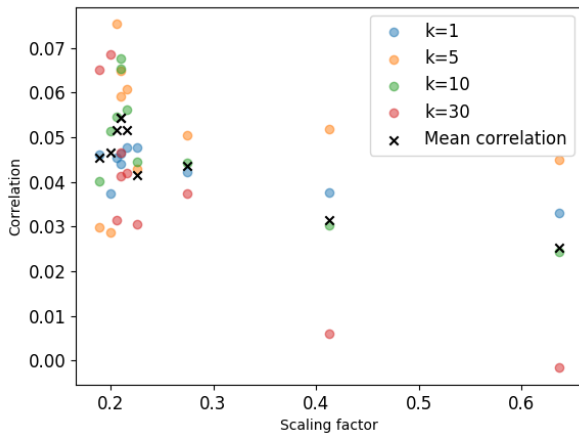


Figure 5: Parameter optimization. Optimization results of the scaling factor s for the Kuramoto global coupling factor c . Colored points show results for different values of k , where each of these points is the mean of 3 repetitions. Black crosses show the average correlation of the tested k values for each value of s .

The optimal scaling factor scales the coupling strength to about one fifth of the original value, which is close to

the ratio of the number of ROIs used in [14] (66) and the Brainnetome atlas (246). This confirms that the optimal coupling strength depends on the number of connections in the connectivity matrix, since it is dependent on the number of ROIs available to connect.

With the optimized scaling factor, simulations for a selection of k values were performed for all patients and resulted in a set of simulated FC matrices for each patient. Example simulations, again using the averaged k -distance matrices over all patients for $k = 1, 5, 25$ (Fig. 6), show some similarities, but also clear differences compared to the empirical averaged FC (Fig. 2 B). While regions of high correlation (e.g. around index 200) are captured by the simulations, the size and distribution of these regions differ significantly. It can also be observed that with increasing k , the simulated FC matrices become more uniform in color, similar to the k -distance matrices (Fig. 3). Regions of high correlation in simulated FC generally seem to have matching regions of low distance in the k -distance matrices. Nevertheless, direct Pearson correlations between the averaged k -distance matrices and the averaged simulated FC matrices returned correlations of -0.355 for $k = 1$, -0.486 for $k = 5$, -0.347 for $k = 25$, showing that even though there are similarities in structure, the simulated FC matrices differ significantly from the k -distance matrices and provide different information.

The simulated FC matrices were also compared to the empirical FC matrices per patient using Pearson correlation (Fig. 7).

Results from simulation contrast those obtained from direct correlation of k -distance matrices with empirical FC (Fig. 4), suggesting that actually not shortest path communication, but communication using k -distance coupling with $k = 8$ achieves the highest mean correlation with empirical FC at $r \approx 0.056$. Now $r > 0$ since we correlate simulated FC with empirical FC. The shortest path coupling ($k = 1$) even has the lowest average correlation of all simulated k , only reaching $r \approx 0.032$. This indicates that actual brain dynamics may not rely solely on shortest path communication, but rather include a higher single digit combination of near-shortest paths around $k = 8$.

In order to further investigate the variability between patients, the best k value (strongest correlation) was determined for each patient, both for the direct k -distance to empirical FC correlation and for the simulated to empirical FC correlation. These were then plotted as histograms (Fig. 8).

For the direct correlation of k -distance matrices with empirical FC (Fig. 8 A), the distribution of best k values peaks strongly at $k = 1$, though with some individuals having optimal correlation around $k = 8$. One individual even has an optimal correlation at $k = 49$, showing how different results can be even in healthy individuals. For the simulated to empirical FC correlation (Fig. 8 B), the distribution is more spread out than in the previous case.

In individual counts, $k = 10$ actually has the highest

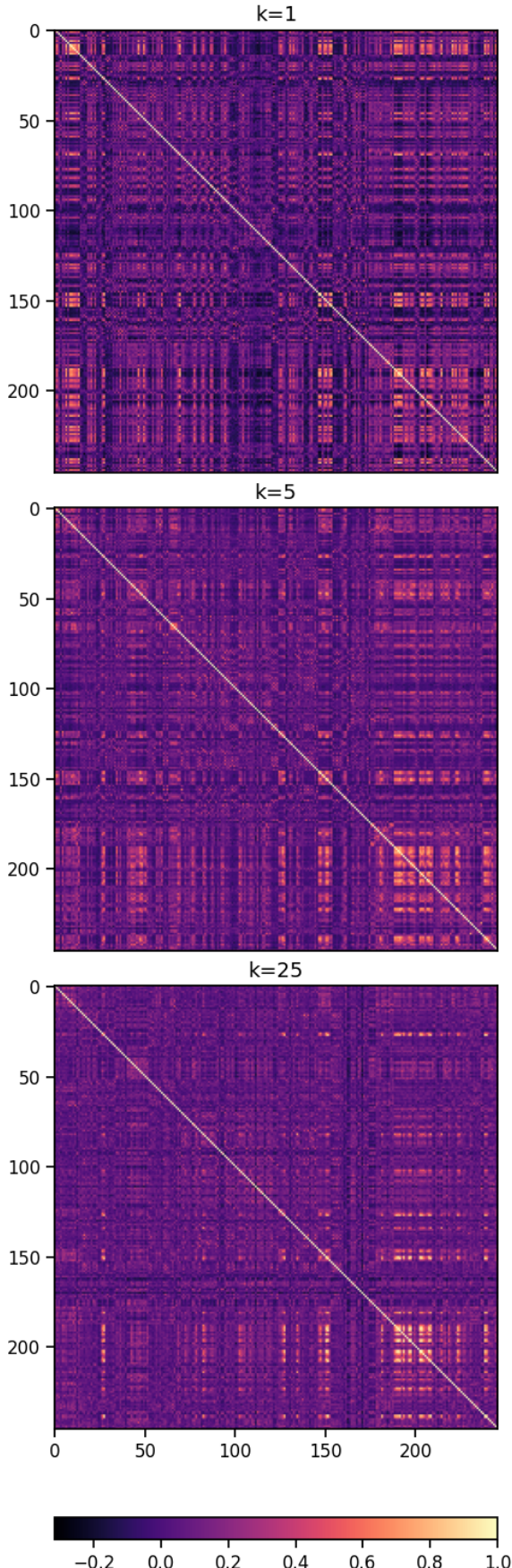


Figure 6: Example FC matrices. Three simulated FC matrices showing $k=1$ (top), $k=5$ (middle) and $k=25$ (bottom), obtained by averaging over all patients. Color describes the functional correlation between two ROIs.

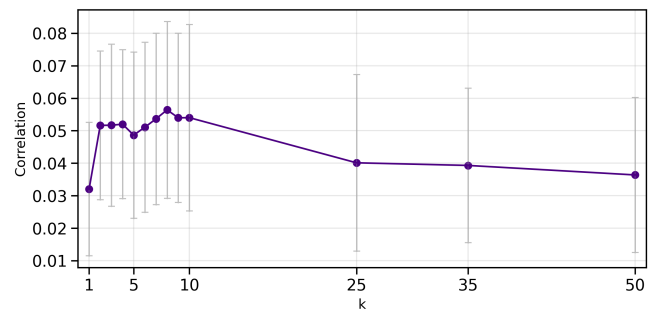


Figure 7: Correlation of simulated FC and empirical FC. Pearson correlation between simulated FC matrices and empirical FC matrices for all patients, shown as mean with standard deviation as error bars.

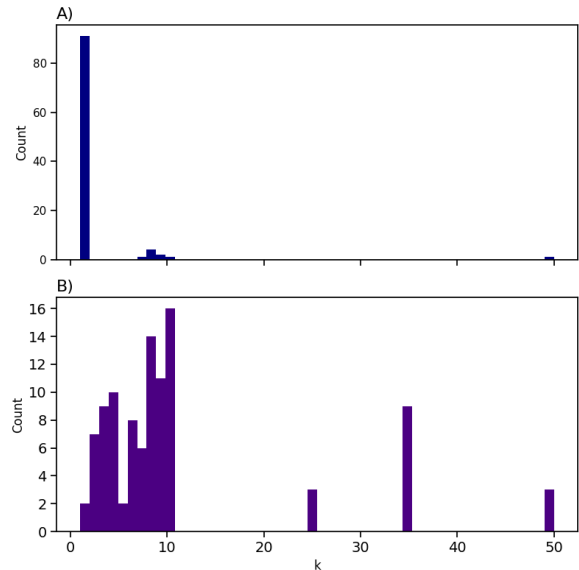


Figure 8: Distribution of best k per patient. Histograms showing the distribution of best k values (strongest correlation) per patient, for the correlation between k -distance matrices and empirical FC (A) and for the correlation between simulated FC and empirical FC (B).

number of patients with optimal correlation, though followed closely by $k = 8$, which had the highest average correlation (Fig. 7). 15 individuals have their optimal correlation at $k = 25, 35$ or 50 , again showing the high variability between individuals.

V. CONCLUSIONS AND OUTLOOK

First and foremost, it is important to note that our results are very limited and should not be given the same weight as more established findings in the field, especially with the low reported correlation values, never exceeding

$|r| = 0.13$. Comparable studies using similar methods have reported higher correlations, e.g. $r = 0.37$ in [15], though they also used different datasets.

Our simulations are much shorter in time than the empirical time series, limiting comparability due to different timescales. We also did not convert the simulated data to BOLD signal, which would be necessary for more accurate comparisons but requires more complicated transformations of the signal using the Balloon-Windkessel hemodynamic model [16].

This very much limits the interpretability of our results, which should be seen as preliminary findings requiring further validation. Nevertheless, some interesting trends can be observed.

Our results regarding the correlation between k -distance matrices and empirical FC suggest that lower values of k have a stronger statistical relationship with functional connectivity than larger k values, with $k = 1$ here even showing strongest mean correlation by far. Simulating brain activity using the Kuramoto model achieved best results on average for $k = 8$, also adding to this sentiment.

Previous work has shown that using logarithmic computation of edge lengths results in the proportion of edges participating in at least one of the k -shortest paths saturating around $k = 5$ [8] [17]. This could suggest that brain communication maximizes the number of edges used for communication while still relying on near-optimal paths for transmission.

Individual patients show high variability in their optimal k values, both for direct k -distance to empirical FC correlation and for simulated to empirical FC correlation. Other work has shown that the SPE model can be used to leverage this variability to actually classify individuals not only in humans, but also macaques and mice [17]. It seems likely that brain communication is highly individual, necessitating personalized models to accurately capture the underlying dynamics.

To further validate our findings, it would be necessary to perform more extensive parameter optimization and

longer simulations, including more k values and longer simulation times to better match empirical data and related work.

If results are confirmed, it would be interesting to investigate further details of k dependence for brain communication. A more thorough investigation of path selection could be performed, e.g. by allowing free combinations between the k -shortest paths instead of the weighted average. Other metrics like quasiperiodic spatiotemporal patterns (QPP) or recurrence quantification analysis (RQA) could be used to evaluate the simulations beyond Pearson correlation of FC matrices, giving a more complete picture of how well the model captures empirical dynamics [15].

In conclusion, our results show interesting potential directions for the improvement of brain communication models, further bridging the gap between pure structural connectivity and functional dynamics through simulation.

VI. CONTRIBUTIONS

Both authors conceptualized the project and drafted section III. D. P. F. drafted sections I and II. L. L. P. wrote the entire code used for the project and drafted sections IV and V. Both authors reviewed and edited the final report.

VII. CONFLICT OF INTEREST

The authors declare that the research was conducted in the absence of any commercial or financial relationships that could be construed as a potential conflict of interest.

VIII. DATA AND CODE AVAILABILITY

Data is available for download at [11]. All source files (code and report) are made publicly available at [18].

-
- [1] A. Avena-Koenigsberger, B. Misic, and O. Sporns, Communication dynamics in complex brain networks, *Nature Reviews Neuroscience* **19**, 17 (2017), relevant because it reviews the importance of network neuroscience to link the structure of the brain with its functional connectivity.
 - [2] D. Bassett and E. Bullmore, Small-world brain networks, *The Neuroscientist : a review journal bringing neurobiology, neurology and psychiatry* **12**, 512 (2007), relevant because it shows the small-world structure of brain networks.
 - [3] M. Heuvel and O. Sporns, Rich-club organization of the human connectome, *The Journal of neuroscience : the official journal of the Society for Neuroscience* **31**, 15775 (2011), relevant because it studies the importance of brain hubs.
 - [4] C. Seguin, O. Sporns, and A. Zalesky, Brain network communication: concepts, models and applications, *Nature Reviews Neuroscience* **24**, 557 (2023), relevant since it describes all the models compared in this project.
 - [5] J. Goñi, M. Heuvel, A. Avena-Koenigsberger, R. Betzel, A. Griffa, P. Hagmann, B. Corominas-Murtra, J.-P. Thiran, and O. Sporns, Resting-brain functional connectivity predicted by analytic measures of network communication, *Proceedings of the National Academy of Sciences of the United States of America* **111**, 833 (2013), relevant because it empirically demonstrates that functional connectivity can be inferred from the brain network structure using network models.

- [6] B. Misic, R. Betzel, A. Nematzadeh, J. Goñi, A. Griffa, P. Hagmann, A. Flammini, Y.-Y. Ahn, and O. Sporns, Cooperative and competitive spreading dynamics on the human connectome, *Neuron* **86**, 1518 (2015), relevant because it studies the application of the linear-threshold model to brain networks.
- [7] A. Avena-Koenigsberger, X. Yan, A. Kolchinsky, M. Heuvel, P. Hagmann, and O. Sporns, A spectrum of routing strategies for brain networks, *PLOS Computational Biology* **15**, e1006833 (2019), relevant because it defines the biased random walk, combining the classical shortest-path communication and the diffusion approach.
- [8] A. Avena-Koenigsberger, B. Misic, R. Hawkins, A. Griffa, P. Hagmann, J. Goñi, and O. Sporns, Path ensembles and a tradeoff between communication efficiency and resilience in the human connectome, *Brain structure and function* **222**, 603 (2017), relevant because it describes the shortest-paths ensemble model, used in this project.
- [9] N. Masuda, M. Porter, and R. Lambiotte, Random walks and diffusion on networks, *Physics Reports* **716**, 1 (2016), relevant because it reviews the model of random walk dynamics in complex networks, such as the brain.
- [10] BioRender.com, Biorender illustration, <https://biorender.com> (2026), relevant because it is the source of an illustration in the method figure.
- [11] Y.-W. Chang, M. Mijalkov, and J. Sun, Brainsimulation, <https://github.com/yu-wei-c/BrainSimulation>, accessed: 2025-11-26. Relevant because it contains the empirical data used for this project.
- [12] L. Fan, H. Li, J. Zhuo, Y. Zhang, J. Wang, L. Chen, Z. Yang, C. Chu, S. Xie, A. R. Laird, *et al.*, The human brainnetome atlas: a new brain atlas based on connectional architecture, *Cerebral cortex* **26**, 3508 (2016), relevant because it describes the brainnetome atlas used in this project.
- [13] P. Virtanen, R. Gommers, T. E. Oliphant, M. Haberland, T. Reddy, D. Cournapeau, E. Burovski, P. Peterson, W. Weckesser, J. Bright, S. J. van der Walt, M. Brett, J. Wilson, K. J. Millman, N. Mayorov, A. R. J. Nelson, E. Jones, R. Kern, E. Larson, C. J. Carey, I. Polat, Y. Feng, E. W. Moore, J. VanderPlas, D. Laxalde, J. Perktold, R. Cimrman, I. Henriksen, E. A. Quintero, C. R. Harris, A. M. Archibald, A. H. Ribeiro, F. Pedregosa, P. van Mulbregt, and SciPy 1.0 Contributors, SciPy 1.0: Fundamental Algorithms for Scientific Computing in Python, *Nature Methods* **17**, 261 (2020), relevant because it is the main library used for computations and analyses in the project.
- [14] J. Cabral, E. Hugues, O. Sporns, and G. Deco, Role of local network oscillations in resting-state functional connectivity, *NeuroImage* **57**, 130 (2011), relevant because it describes the Kuramoto model and parameters used in this project.
- [15] A. Kashyap and S. Keilholz, Dynamic properties of simulated brain network models and empirical resting state data, *Network Neuroscience* **3**, 1 (2018).
- [16] K. J. Friston, L. Harrison, and W. Penny, Dynamic causal modelling, *Neuroimage* **19**, 1273 (2003).
- [17] A. Griffa, M. Mach, J. Dedelley, D. Gutierrez-Barragan, A. Gozzi, G. Allali, J. Grandjean, D. Van De Ville, and E. Amico, Evidence for increased parallel information transmission in human brain networks compared to macaques and male mice, *Nature Communications* **14** (2023).
- [18] L. Prader and D. P. Fonseca, Project github repository, https://github.com/luprader/project_SOCS, relevant because it contains all the code and report used for the project.